Annals of Warsaw University of Life Sciences-SGGW
Forestry and Wood Technology № 119, 2022: 94-103
(Ann. WULS-SGGW, For. and Wood Technol. 119, 2022: 94-103)

Raman mapping as a characterisation tool of carbon in indexable knives for wood-based materials machining

MAREK BARLAK[1], MAGDALENA WILCZOPOLSKA[1], JACEK WILKOWSKI[2], ZBIGNIEW WERNER[1], JERZY ZAGÓRSKI[1]

[1] Plasma/Ion Beam Technology Division, Material Physics Department, National Centre for Nuclear Research Świerk,
[2] Department of Mechanical Processing of Wood, Institute of Wood Sciences and Furniture, Warsaw University of Life Sciences,

Abstract: *Raman mapping as a characterisation tool for carbon in indexable knives for wood-based materials machining.* This work reports the results of Raman Spectroscopy analysis of the virgin and the modified WC-Co indexable knives. The conducted studies focused on characterising structural changes after ion implantation of samples by rhenium and lead. The presented results of single spectra and maps of samples showed that the Raman Spectroscopy method allows one to detect changes in the structure after modification of WC-Co indexable knives for wood-based materials machining. The reported changes have been discussed and assigned to changes in characteristic Raman bands.

Keywords: Raman spectroscopy, Raman mapping, WC-Co indexable knives, tool modification

INTRODUCTION

Cemented tungsten carbides – a combination of hard and brittle carbides and a relatively soft and ductile metallic binder – give rise to an exceptional combination of attractive properties such as strength, hardness, fracture toughness, refractoriness, stiffness, resistance to compressive deformation and wear resistance at room temperature, as well as at higher temperatures up to 400°C (Milman et al., 1997, Sheikh-Ahmad and Bailey 1999, Pirso et al., 2004, Bonny et al., 2010, Choi et al., 2010, Olovsjö et al., 2013). Unfortunately, the durability of the tools made of this material is still insufficient. There are several methods to improve this property, ion implantation being one of them (Barlak et al., 2016, Barlak et al., 2017).

Apart from developments of modifications, the methods of a quick evaluation of the obtained results are sought. Raman spectroscopy (Wilczopolska et al., 2021) seems to be a potential, ultrafast and non-destructive method which can be used for this purpose. It is a method in which a laser generates the incident radiation. It is assumed that the incident radiation excites the molecules of the analysed substance to some virtual energy level, from which they return to the ground state by emitting photons of scattered radiation of different frequencies. The Raman spectrum shows a dependence of the signal intensity on frequency, which is the difference between the frequencies of the incident radiation and the scattered radiation (Raman shift). The spectral analysis provides information about the molecule's structure (i.e., about the interconnection of atoms in the molecule (Smith 2005)).

The Raman technique of WC-Co indexable knives is not widely described in the literature. Describing bands from WC-Co is often possible when there are metal-ceramic composite or cermet coatings. Unfortunately, in the case of knives, these bands are not visible due to high fluorescence caused by metal.

The situation is different for the presence of carbon in the material microstructure. Raman spectroscopy is one of the most sensitive and informative techniques characterising disturbances in carbon materials (Xu et al., 2020, Gordon and McGoverin 2011).

According to the literature, Raman spectra of carbon materials can be characterised by two main bands: the G band (located at about 1,590 cm^{-1}), where the letter G refers to graphite and the D band (located at about 1,350 cm^{-1}), where "D" relates to a defect. A significant relationship between the bands is the intensity ratio of I_D/I_G. An increase in the number of defects is manifested by an increase in the intensity of the D-band (I_D) on the Raman spectrum and, thus, an increase in the intensity ratio I_D/I_G (Härmas et al., 2021). Raman spectra provide information on the degree of structural order when carbon is analysed without the need to refer to other techniques.

The idea of our investigations is an attempt to determine a functional feature of the modified tools (e.g., their durability) using non-destructive methods (e.g., Raman spectroscopy). It is an important aspect in the durability of tools. In our previous paper (Barlak et al., 2021), we demonstrated the potential relationship between the existence of D, G or D+G peaks and the durability of WC-Co tools for wood-based materials machining treated using three different methods. In the current work, an attempt is made to analyse the carbon content in the samples, ion implanted with rhenium (the element for high-temperature applications) and lead (the "lubricating" element), in comparison to the virgin material. Additionally, this paper briefly describes the characterisation tool in the form of Raman mapping analysis of all investigated cases.

MATERIALS AND METHODS

The commercially available WC-Co indexable knives – produced by Ceratizit company (KCR08), with dimensions of 29.5×12×1.5 mm^3 and presented in Figure 1 – were used in the investigations.

The clearance surfaces of the investigated knives were ion implanted with rhenium and lead, using an ion implanter without mass separation, described in detail in the paper of (Nikolaev and Ozur 2014). The implanted dose of the implanted ions was 1e17 cm^{-2}, and the acceleration voltage was 50 kV in all cases.

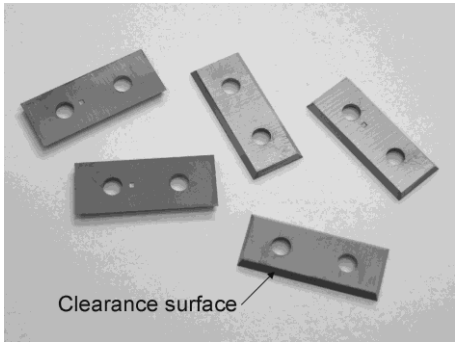

Figure 1. WC-Co indexable knives

The ion beam generated by an ion implanter without mass separation contains several kinds of ions with different degrees of ionisation. Additionally, the percentage shares of individual ion types are also different. The use of all data for the selected element is usually cumbersome; therefore, the average charge state (ACS) is a more popular parameter for the calculation/modelling as an equivalent of the sum of the profiles for the individual ion kinds (Barlak et al., 2019). Table 1 shows the percentage charge state

distribution and average charge state of rhenium and lead.

Table 1. The percentage charge state distribution and average charge state of rhenium and lead (Krivonosienko et al., 2001, Barlak et al., 2019)

Implanted ions	Ion energy for acceleration voltage of 50 kV (keV)					Average charge state
	50	100	150	200	250	
	Percentage charge state distribution (%)					
	1+	2+	3+	4+	5+	
$Re^{+} + Re^{2+} + Re^{3+} + Re^{4+} + Re^{5+}$	2	26	40	26	3	3.0
$Pb^{+} + Pb^{2+}$	40	60	-	-	-	1.6

The processes of ion implantation were preceded by modelling. The Stopping and Range of Ions in Matter (SRIM-2013.00 (SRIM 2021)) freeware type code was used for the modelling of the shapes of the depth profiles of the implanted elements in W-C-Co substrate material (modelling codes treat the sample as a set of atoms that do not form chemical compounds), and the main atomic parameters are used.

The modelling was performed for 100,000 implanted ions. W-C-Co of a composition: 90.86% of tungsten, 5.94% of carbon and 3.2% of cobalt by weight per cent; 47.4% of tungsten, 47.4% of carbon and 5.2% of cobalt by atomic per cent was defined as a target. Its density, adopted for the simulation, was 15.2 g/cm^3. This value was declared by the knife supplier (KCR08-type knives by Ceratizit, Austria).

The simulations were performed at room temperature and for the total implanted fluence of 1e17 cm^{-2}, including percentage charge state distribution data from Table 1. The acceleration voltage was 50 kV. The modelling did not take into account the phenomenon of substrate sputtering by the implanted ions.

In the next step, the virgin (non-modified, non-treated) and treated (implanted) knives were analysed using Raman spectroscopy. The measurements of Raman spectroscopy were recorded using a WITec confocal Raman microscope (Alpha 300R, WITec, Germany) with a high-power frequency-doubled Nd:YAG laser emitting a green excitation wavelength of 532 nm. A WITEC UHTS VIS-NIR spectrometer was equipped with a CCD detector (cooled to -60°C). Raman Stokes signals were recorded with an objective lens with a magnification of 100× (Zeiss LD EC Epiplan-Neofluar Dic 100×/0.75). The spectra were collected over a wavenumber range of 70 to 3,500 cm^{-1}, with an integration time of 10 s for measurements of a single spectrum and 5 s for image mapping. Mapping capability is provided by an automated x-y stage where the sample is placed. Raman image mapping was performed by scanning over an area of 20×20 μm^2. The software collects all spectra made by scanning samples in two spatial directions (X and Y) point by point and line by line to generate a 2D image. The measurements of the Raman spectrum were made every 0.5 μm from each pixel (the effective spot size used on the sample was 0.7 μm) in 40 lines. The results were analysed using WITec Project software.

RESULTS AND DISCUSSION

Figure 2 shows the results of modelling the ion implantation of rhenium and lead to W-C-Co substrate material, without accounting for sputtering, for rhenium with five charge state ions and rhenium with two ones, and for the acceleration voltage of 50 kV.

The profiles, named $Re^{+} + Re^{2+} + Re^{3+} + Re^{4+} + Re^{5+}$ and $Pb^{+} + Pb^{2+}$, were modelled for the implantation without mass separation. The profiles ACS are the

equivalent of the previous profiles modelled for the average charge state. The single profiles – Re^{+}, Re^{2+}, Re^{3+}, Re^{4+} and Re^{5+} for rhenium and Pb^{+} and Pb^{2+} for lead – were modelled for the individual charge state and the percentage share in the ion beam. The sum of these individual profiles should give the required profile of $Re^{+} + Re^{2+} + Re^{3+} + Re^{4+} + Re^{5+}$ or $Pb^{+} + Pb^{2+}$.

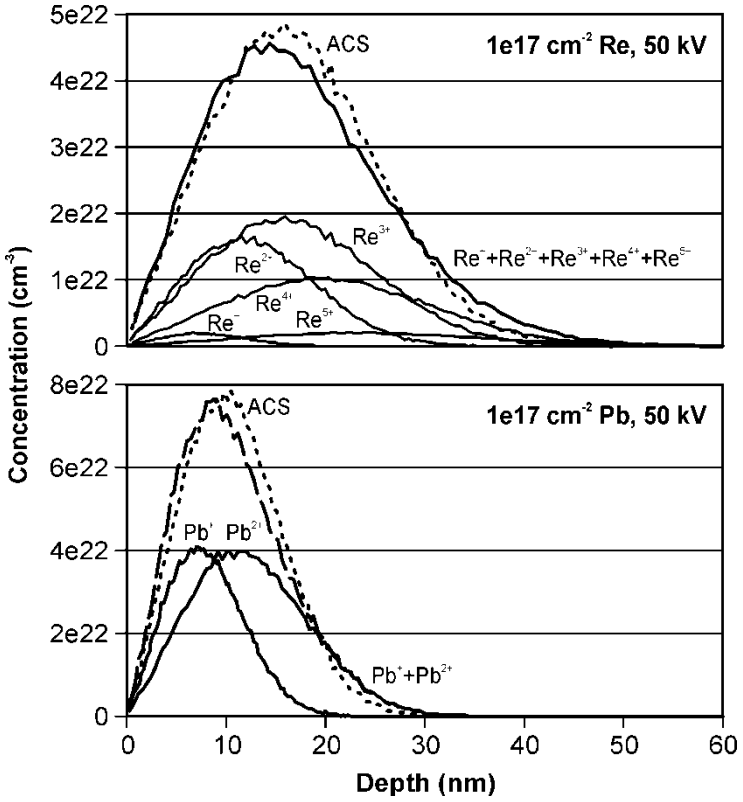

Figure 2. The modelled depth profiles for the ion implantation of rhenium and lead to W-C-Co substrate

The values of the main peak parameters (i.e., peak volume dopant concentrations N_{max}, the projected range R_p, the range straggling ΔR_p, the kurtosis and the skewness) determined for rhenium and lead profiles (rounded to two decimal places) are presented in Table 2. The bold data is for the modelling of the case of the ion implantation using the ion beams without mass separation.

We can see that the peak volume dopant concentrations is about 1.7 times more for lead in comparison to rhenium. The values of the projected range and the range straggling are about 1.6 times more for rhenium compared to lead. The values of the kurtosis and skewness are similar for both described cases. The difference is at a level of a few per cent. The calculated values of sputtering yield for the ACS case, using SUSPRE code (SUSPRE 2021), are 11.76 atoms/ion for rhenium and 10.47 atoms/ion for lead.

In the next step, the virgin and the modified samples were investigated using Raman spectroscopy. The Raman mapping technique allows us to obtain statistics and study a variation of the Raman shift in one mapping. To obtain a complete picture of the carbon distribution, mapping images from their characteristic peaks were made (Figures 3-5). These figures present a map of the Raman shift of the main characteristic carbon bands D and G. The mapping image was generated by the software based on Lorentz fit of the

two peaks of the G and D bands. The Voight function was not used due to software limitations. Background noise was effectively removed as noise by off-setting the baseline of the collected Raman spectra.

By analysing the colour scale bar, one can determine band shifts prevailing in the individual samples and estimate the sample homogeneity. In the unmodified virgin sample (Figure 3), the predominant bands are located at ~1,354 cm^{-1} for the D band and at 1,589 cm^{-1} for the G band.

Table 2. The values of the main peak parameters for rhenium and lead implanted ions

Implanted ions	Peak parameter				
	N_{max}(cm^{-3})	R_p(nm)	ΔR_p(nm)	kurtosis	skewness
Re^{+}	2.03e21	8.2	8	1.79	0.68
Re^{2+}	1.65e22	12.8	12.4	2.89	0.42
Re^{3+}	1.94e22	17	16	2.51	0.46
Re^{4+}	1.03e22	20.9	19.6	2.22	0.49
Re^{5+}	2.04e21	24.7	22.8	2.82	0.34
Re^{+} + Re^{2+} + Re^{3+} + Re^{4+} + Re^{5+}	**4.57e22**	**17.2**	**18**	**3.53**	**0.71**
ACS for Re	4.86e22	17	16	2.89	0.39
Pb^{+}	4.1e22	8	7.6	2.46	0.54
Pb^{2+}	3.98e22	12.4	11.6	2.94	0.42
Pb^{+} + Pb^{2+}	**7.66e22**	**10.6**	**11**	**3.32**	**0.68**
ACS for Pb	7.85e22	10.7	10	2.96	0.43

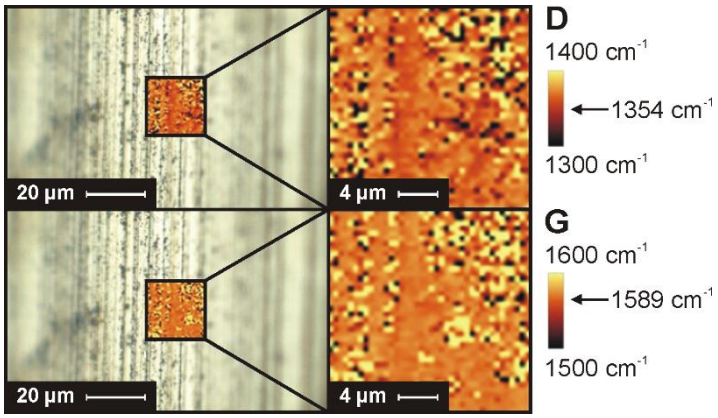

Figure 3. Maps of D and G peak positions of the virgin sample

Ion implantation results in shifting the wavenumber, as shown in Figures 4 and 5. In the case of rhenium, the ion implantation D band is shifted to a higher wavenumber and the G band to a lower wavenumber. In the case of samples implanted with lead ions, the D band is shifted to lower values and the G band to higher values compared to the untreated sample.

The Raman spectra of the most frequently occurring Raman bands in the maps of virgin, Re, and Pb implanted samples of WC-Co material are presented in Figure 6. The entire spectrum obtained on a Confocal Raman Microscope is presented on the left side. However, considering changes in the material as far as carbon is concerned, the focus is on the spectral range from 1,000 to 2,000 cm^{-1}.

As mentioned above, the analysis of individual bands of WC-C is impossible due to high metal fluorescence. However, it is possible to focus on the interpretation of carbon

that changes through ion implantation. A broad, diffused and intense fluorescence signal was removed by background subtraction. The problem is that the background photoluminescence can be so high that the noise generated by this signal interferes with measuring quantitative parameters of the Raman bands.

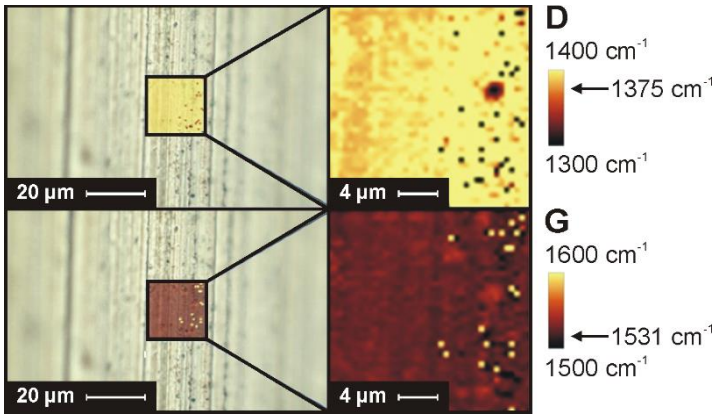

Figure 4. Maps of D and G peak positions of the Re implanted sample

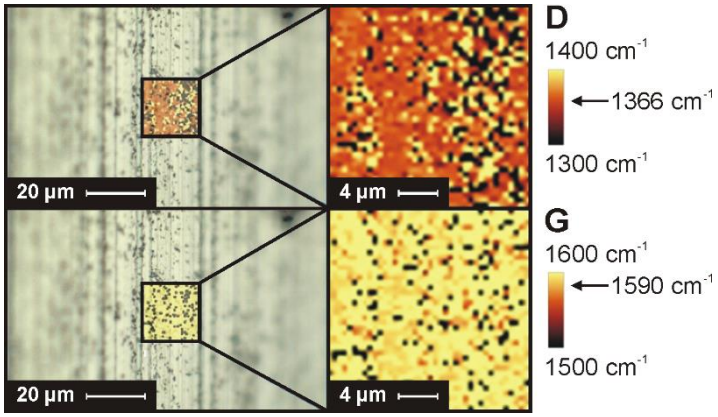

Figure 5. Maps of D and G peak positions of the Pb implanted sample

This is why peaks' position intensities, FWHM (full width at half maximum), and shapes were optimised by Fityk 1.3.1 code (Fityk 2021) using the Voight function.

Table 3. The quantitative parameters of characteristic Raman peaks of the virgin, Re-, and Pb-implanted samples.

Sample	D			G			I_D/I_G
	Raman shift (cm^{-1})	Intensity	FWHM (cm^{-1})	Raman Shift (cm^{-1})	Intensity	FWHM (cm^{-1})	
Virgin	1354	977	117	1589	1135	113	0,86
Re	1375	679	189	1531	702	141	0,97
Pb	1366	1018	161	1590	1195	109	0,85

In the case of disordered and/or partially graphitised carbons, the Raman spectrum features more vibrational bands than the D and the G band. In Figure 6 (lower right), extra Voight functions – marked by dashed lines – are added to obtain a reasonable fit of the disordered carbon spectra. These bands originate from the highly disordered areas,

resulting in softening of the photon modes. However, they are not taken into account in the case of the Raman spectra analysis.

As can be seen from Figure 6, an already virgin sample can be characterised by an amorphous regime of carbon because of its characteristic broad line. Table 3 shows the results of the fitted Raman bands.

The Raman spectrum provides a lot of information about the analysed material. The analysis of the Raman mode wave numbers, widths and intensities allows one to obtain information about the compositions, chemical environment, bonding and crystalline/amorphous structure of a sample material.

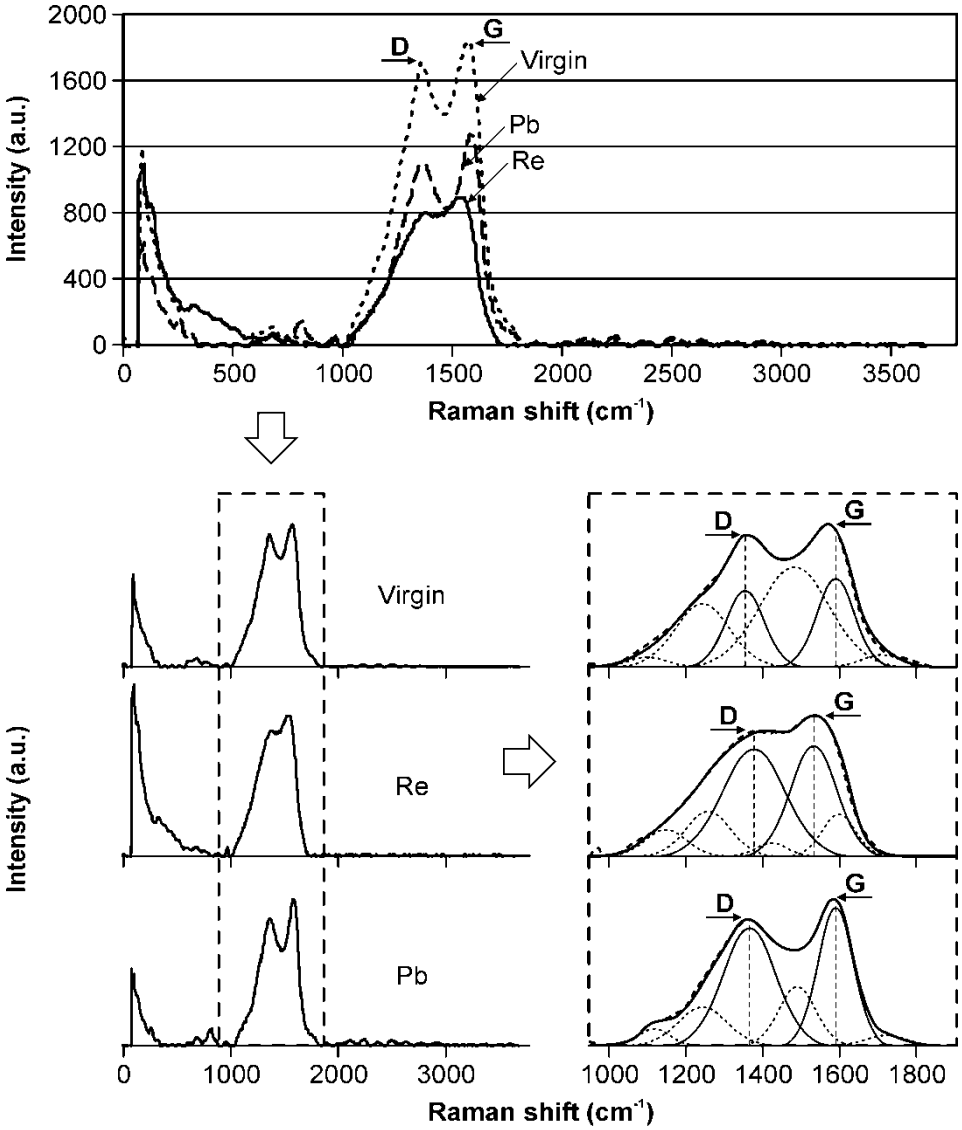

Figure 6. Raman spectra of virgin, Re, and Pb implanted samples in comparison with spectrum fitted with Voight functions

The characteristic Raman frequencies reflect a material composition. Considering the width changes of the Raman peak, conclusions can be drawn about the quality of the crystal. The FWHM informs whether the layer is crystalline or amorphous because Raman scattering is sensitive to the degree of crystallinity in the sample. Typically, a crystalline material yields a spectrum with very sharp, intense Raman peaks, while

an amorphous material will show broader, less intense Raman peaks. Rhenium ion implantation resulted in the least ordered carbon. It is most likely related to the degree of material defects. Both the D and G bands are very wide and have equivalent intensities. Lead ion implantation resulted in more ordered material, where the higher wavenumber band becomes narrower, whereas the D band remains very wide. All the samples exhibited the broad asymmetric line shape characteristic of the amorphous material. Taking into account Raman shift changes, ion implantation results in significant changes in the frequency of the Raman peak. Depending on the applied ions, there are deviations in wavenumber. Re ions cause significant structural changes which can be deduced from the shift of the D band to higher, and the G band to lower wavenumber. Regarding Pb ion implantation, the Raman spectrum is shifted to a higher wavenumber than in the virgin sample, which leads to conclusions that these ions can be the reason for subtle structural changes.

The intensity of a spectrum is directly proportional to concentration. Taking into account the intensities ratio, the sample implanted by rhenium ions shows an increase compared to the non-implanted sample, which means an increase in the number of defects. Lead ion implantation results in a slight decrease in the I_D/I_G ratio with respect to the virgin sample. This is related to an increasing ordering of the carbon structure after ion implantation.

CONCLUSIONS

Summarising the preliminary investigations, one may conclude that rhenium and lead (located quite close to one another in the periodic table and differing by only 10% as regards the atomic mass) affect the structure of the implanted WC-Co in different ways. Re implantation seems to affect the material structure more effectively than the Pb one. The detected values of FWHM of the Raman peaks indicate that the Re implanted material is more amorphous (an increase of the FWHM value by more than 60% for the D band and about 25% for the G band with respect to the virgin material), while that implanted with Pb is more crystalline (the FWHM increase by over 35% for D band and the FWHM decrease by about 1% for G band). Similarly, the I_D/I_G intensity ratio, linked to the carbon structure crystallinity, points to better crystallinity of the lead implanted material (a decrease of I_D/I_G by over 1%). For Re ion implantation, this value increases by almost 13%.

The presented research will be continued, and an attempt will be made to correlate the presented results with the wear investigations.

REFERENCES

1. BARLAK M., WILKOWSKI J., WERNER Z., 2016: Ion implantation changes of tribological and corrosion resistance properties of materials used in wood industry, Annals of Warsaw University of Life Science - SGGW, Forestry and Wood Technology 94, 19-27.
2. BARLAK M., WILKOWSKI J., BORUSZEWSKI P., WERNER Z., PAŁUBICKI B., 2017: Changes of functional properties of materials used in wood industry after ion implantation processes, Annals of Warsaw University of Life Science - SGGW, Forestry and Wood Technology 97, 133-139.
3. BARLAK M., WILKOWSKI J., WERNER Z., 2019: Modelling of nitrogen implantation processes into WC-Co indexable knives for wood-based material machining using ion implanters with or without direct ion beam, Annals of Warsaw University of Life Science - SGGW, Forestry and Wood Technology 108, 68-78.

4. BARLAK M., WILKOWSKI J. WILCZOPOLSKA M., WERNER Z., STASZKIEWICZ B., ZAGÓRSKI J., 2021: Raman Spectroscopy in the investigations of indexable knives for wood-based materials machining, Annals of Warsaw University of Life Sciences - SGGW, Forestry and Wood Technology 114, 33-42. DOI: 10.5604/01.3001.0015.2371
5. BONNY K., DE BAETS P., PEREZ Y., VLEUGELS J., LAUWERS B., 2010: Friction and wear characteristics of WC-Co cemented carbides in dry reciprocating sliding contact, Wear 268, 1504-1517.
6. CHOI S.-H., KANG S.-D., KWON Y.S., LIM S.G., CHO K.K., AHN I.-S., 2010: The effect of sintering conditions on the properties of WC-10wt%Co PIM compacts, Research on Chemical Intermediates 36, 743-748.
7. FITYK. Curve fitting and peak fitting software, https://fityk.nieto.pl/
8. GORDON K.C., McGOVERIN C.M., 2011: Raman mapping of pharmaceuticals, International Journal of Pharmaceutics 417, 151-162. DOI: 10.1016/j.ijpharm.2010.12.030
9. HÄRMAS R., PALM R., KURIG H., PUUSEPP L., PFAFF T., ROMANN T., ARUVÄLI J., TALLO I., THOMBERG T., JÄNES A., LUST E., 2021: Carbide-derived carbons: WAXS and Raman spectra for detailed structural analysis, Materials 7, 29. DOI: 10.3390/c7010029
10. KRIVONOSIENKO A.W., NIKOLAEV A.G., LI S., 2001: Технические описание и инструкция по эксплуатации ионного источника "Титан-3" (Technical descriptions and operating instructions of the ion source "Titan-3"), Российская Академия Наук - Институт Сильноточной Электроники, Tomsk, in Russian.
11. MILMAN. YU.V., CHUGUNOVA S., GONCHARUCK V., LUYCKX S., NORTHROP I.T., 1997: Low and high temperature hardness of WC-6 wt% Co alloys. International Journal of Refractory Metals and Hard Materials 15, 97-101.
12. NIKOLAEV A.G., OZUR G.E., 2014: Сильноточный ионный имплантер прямого действия типа «МЕВВА-РИТМ» (MEVVA-RITM) с возможностью обработки мишени нмпульсным электронным пучком (Технические описание и руководство по эксплуатации), Институт Сильноточной Электроники СО РАН, Tomsk, in Russian.
13. OLOVSJÖ S., JOHANSON R., FALSAFI F., BEXELL U., OLSSON M., 2013: Surface failure and wear of cemented carbide rock drill buttons - The importance of sample preparation and optimised microscopy settings, Wear 302, 1546-1554.
14. PIRSO J., LETUNOVITŠ S., VILJUS M., 2004: Friction and wear behaviour of cemented carbides, Wear 257, 257-265.
15. SHEIKH-AHMAD J.Y., BAILEY J.A., 1999: High-temperature wear of cemented tungsten carbide tools while machining particleboard and fiberboard. Journal of Wood Science 45, 445-455.
16. SMITH, E., DENT, G., 2005: Modern Raman Spectroscopy - A practical approach, John Wiley & Sons Ltd, Chichester. DOI:10.1002/0470011831
17. SRIM. Interactions of ions with matter, http://www.srim.org/
18. SUSPRE. Implantation calculator code, https://uknibc.co.uk/SUSPRE/
19. WILCZOPOLSKA M., NOWAKOWSKA-LANGIER K., OKRASA S., SKOWRONSKI L., MINIKAYEV R., STRZELECKI G.W., CHODUN R., ZDUNEK K., 2021: Synthesis of copper nitride layers by the Pulsed Magnetron

Sputtering method carried out under various operating conditions, Materials 14, 2694. DOI: 10.3390/ma14102694
20. XU J., LIU J., ZHANG L., ZHANG, XIN L., PENG X., KAI H., LIMO S., SHENG W., YI H., SONG X., 2020: Chemical imaging of coal in micro-scale with Raman mapping technology, Fuel 264, 116826. DOI: 10.1016/j.fuel.2019.116826

Streszczenie: *Mapowanie Ramana jako narzędzie do charakteryzowania węgla w wymiennych nożach do obróbki materiałów drewnopochodnych*. W pracy przedstawiono wyniki analizy wyjściowych i modyfikowanych wymiennych noży WC-Co, metodą spektroskopii ramanowskiej. Prowadzone badania koncentrowały się na charakterystyce zmian strukturalnych po implantacji próbek jonami renu i ołowiu. Przedstawione wyniki badań na spektroskopie Ramana w postaci pojedynczych widm i dwuwymiarowych płaszczyzn wykonanych na podstawie pojedynczych widm wykazały, że metoda spektroskopii Ramana umożliwia obserwowanie zmian w strukturze modyfikowanych wymiennych noży WC-Co do obróbki materiałów drewnopochodnych. Zaobserwowane zmiany zostały omówione i przypisane odchyleniom charakterystycznych pasm Ramana.

Corresponding author:

Jacek Wilkowski
e-mail: jacek_wilkowski@sggw.edu.pl
Warsaw University of Life Sciences - SGGW
Institute of Wood Sciences and Furniture
Department of Mechanical Processing of Wood
159 Nowoursynowska St.
02-776 Warsaw, Poland